Theoretical and Applied Climatology
https://doi.org/10.1007/s00704-024-05157-5

RESEARCH

Sensitivity analysis of streamflow parameters with SWAT calibrated by NCEP CFSR and future runoff assessment with developed Monte Carlo model

Seyedeh Hadis Moghadam[1] · Parisa-Sadat Ashofteh[1,2] · Vijay P. Singh[3]

Received: 9 July 2023 / Accepted: 15 August 2024

Abstract
The present study analyzed sensitivity of flow parameters using SWAT and effect of climate change on surface water resources, considering uncertainty with Monte Carlo. For this purpose, output of nine-model related to fifth-climate change-report during baseline period 1971–2000 was weighted. Using Monte Carlo, 100 samples of probabilistic distribution of basin temperature and rainfall were generated. LARS-WG model was used for downscaling, then temperature and precipitation were calculated under RCP2.6 and RCP8.5 for future periods 2040–2069 and 2070–2099. SWAT was calibrated using observational-data and the National Centers for Environmental Prediction (NCEP) Climate Forecast System Reanalysis (CFSR) (NCEP CFSR) global climate datasets and sensitivity of parameters affecting flow was analyzed. Results showed that observed-data had better performance than NCEP CFSR. Finally, future runoff was calculated under RCP2.6 and RCP8.5 for 2040–2069 and 2070–2099. Results showed that average annual runoff decreased by 84, 80, 82 and 80%, for 2040–2069 (RCP2.6 and RCP8.5) and for 2070–2099 (RCP2.6 and RCP8.5) relative to baseline, respectively.

1 Introduction

Optimal management of water resources is being emphasized through application of new and efficient technologies in simulating water resources components and use of hydrological models, and application of methods to reduce water shortage stress in the demand sector. Sustainable management of water resources, especially in arid and semi-arid regions, requires the determination of water balance components (Porhemmat et al. 2018). Determination of each component has been done using various methods, such as hydrological modeling, remote sensing, and geographic information system (GIS).

Hydrological models are able to simulate various hydrological processes and using different hydrological models, studies have been conducted, some of which are mentioned. Mishra et al. (2007) simulated runoff and sediment on a daily and monthly scale in a small basin in India using the SWAT model. R^2 and Nash-Sutcliffe efficiency coefficient (NSE) values for daily runoff in the model calibration period were 0.93 and 0.70, respectively. For monthly runoff in the model calibration period, the values of these two coefficients were 0.99. During the validation period, the R2 coefficient and NSE coefficient values were 0.78 and 0.60 for daily runoff and 0.92 and 0.88 for monthly runoff, respectively. Te Linde et al. (2008) compared the performance of two rainfall-runoff models of hydrologiska byrans vattenavdelning (HBV) and semi-distributive variable infiltration capacity (VIC) in the Rhine catchment. To investigate the effect of climate change on the outflow of the basin, it was necessary to select the hydrological model with the best performance. The results showed that the conceptual semi-distributive model (HBV) performs better than the distributed land surface

✉ Parisa-Sadat Ashofteh
ps.ashofteh@qom.ac.ir

Seyedeh Hadis Moghadam
sh.moghadam@stu.qom.ac.ir

Vijay P. Singh
vsingh@tamu.edu

[1] Department of Civil Engineering, University of Qom, Qom, Iran

[2] Center of Environmental Research, University of Qom, Qom, Iran

[3] Department of Biological and Agricultural Engineering, Zachry Department of Civil & Environmental Engineering, Texas A&M University, College Station, TX, USA

Published online: 29 August 2024

model (VIC). Li and Zhang (2008) compared the performance of distributive hydrological models for flood simulation in the Yellow river sub-basins. The results showed that the three models used had the ability to simulate floods in the basin and could be used to predict floods in the basin. Among the three models used, the GTOPMODEL based GIS model showed the best performance in the simulations. Ghavidelfar et al. (2011) compared the performance of the quasi-distributed model ModClark and the lumped parameter model Clark. This study was performed for the Randan basin of semi-arid basins in the southwest of Tehran, because ModClark is a raster model and its output results were more acceptable in the calibration stage. The results showed that both models had acceptable results for rainfall-runoff simulation in this basin. However, the quasi-distributed ModClark model showed better results due to the spatial distribution parameters. Oeurng et al. (2011) used the SWAT model in a large basin with an area of 110 square kilometers located in southwestern France to simulate runoff and sediment in this basin. The study results showed that the SWAT model was able to simulate runoff and sediment in large basins properly. Sommerlot et al. (2013) used a comparative study to compare the accuracy of three hydrological models SWAT, high impact targeting (HIT), and revised universal soil loss equation (RUSLE2) in basin-scale hydrological simulations with P-factor and R-factor statistics. The results showed that the SWAT model with P-factor equal to 0.51 and R-factor equal to 0.31 had the highest accuracy amongst the three models. Zuo et al. (2016) investigated the effects of climate change and land use on runoff and sediment in the Huangfuchuan river basin in China using the SWAT model. The results showed a decrease in annual runoff and sediment in this basin due to changes in rainfall and temperature and land use changes. This decrease in runoff and sediment in the upstream area of the river was much more than downstream. Moghadam et al. (2023b) compared data mining, lumped, and distributed models to assess climate change effects on surface water resources in Iran's Sanjabi basin. They used 17 climate models and evaluated their performance criteria. The CNRM-CM5 model outperformed others in rainfall, average temperature, and minimum temperature projections, while GFDL-CM3 excelled in maximum temperature projections. LARS-WG was the most predictive downscaling method. Among the models tested for future runoff projection, IHACRES performed best, showing a reduction in runoff under all emission scenarios. Notably, runoff decreased by 42.0% and 44.3% in the periods 2040–2069 and 2070–2099, respectively, under the RCP8.5 scenario.

Also, temporal and spatial changes of precipitation in the hydrological models using reanalysis climate datasets are of interest to researchers. Studies have shown that climatic data has been widely used in the SWAT model. Among these researches, the following can be mentioned. Dile and Srinivasan (2014) by examining NCEP CFSR data and comparing them with observational data in different and large areas in the Nile catchment area whose observational data was low density, concluded that there was no significant difference between these data. Fuka et al. (2014) compared NCEP CFSR data and observations. This study concluded that the NCEP CFSR data performed better than the observational data in simulating river flow. Monteiro et al. (2016) compared ERA and NCEP CFSR databases with observational data in a simulation of a basin in Brazil. The results showed that the combination of these three databases could improve the simulation accuracy well.

Also, marked changes in temperature and precipitation patterns greatly impact the quantity and quality of water resources. So, runoff estimation and evaluating water resources under climate change and for future periods are necessary.

Investigating the impact of climate change and land use in the Hoeya River basin in South Korea under RCP greenhouse gas scenarios, Kim et al. (2013) showed that although the impact of land-use change was less than climate change, these changes can increase the seasonal diversity in the river basin runoff due to climate change. Park et al. (2015) predicted drought in South Korea in the period (2014–2100) under RCP climate change scenarios and showed that the most severe drought throughout the 87-year period with the minimum effective drought index (EDI) of −3.54 with a duration of 560 days would occur in the period 2039–2041. Su et al. (2015) evaluated possible changes in precipitation and flow in the Songhuajiang River basin in China by considering ECHAM5 climatic conditions under A2, B1 and A1B scenarios and CMPI5 models under RCP2.6, RCP4.5 and RCP8.5 scenarios in the period 2011–2050. They showed that precipitation under RCP scenarios increased more than under SRES scenarios. Santini and Paola (2015) examined changes in the discharge of the Mad River in New York using current and future climate zoning under the CMCC-CM model and the RCP4.5 and RCP8.5 scenarios, and showed that the climate of cold and polar regions with a moderate and increasing trend was becoming a dry and tropical climate. Moghadam et al. (2023a) studied climate change impacts on surface water and groundwater usage in Iran's Khorramabad basin. They analyzed temperature and rainfall data under different emission scenarios, projecting decreased water resources and groundwater levels. Using a conjunctive operation model, they assessed potential water supply deficits, emphasizing the need for adaptive management strategies amidst changing climatic conditions. Kalhori et al. (2023) developed the Multi-Objective Invasive Weed Optimization Algorithm (MOIWOA) for optimizing

water allocation in the face of climate change. They verified the algorithm's efficacy through benchmark functions, comparing its results with those from MOPSO and NSGA-II. Subsequently, they applied MOIWOA to allocate water for drinking, industrial, and agricultural purposes, aiming to maximize the reliability and resiliency indexes of water supply systems. The model effectively reduced failure periods and allocated water efficiently, particularly during hot months. Under the RCP85 climate change scenario for 2070–2099, they observed an 11% increase in reliability and a 66% increase in resiliency. The researchers employed Gray Relationship Analysis (GRA) to select the best solution from the Pareto solutions and prioritize multi-objective solutions based on Gray Relational Grade (GRG).

On the other hand, climate models have uncertainty, which has been conducted in different studies. Prudhomme et al. (2003) described a methodology for quantifying uncertainties of climate change impacts. Uncertainties were calculated with a set of 25,000 climate scenarios randomly generated by Monte Carlo simulation, and employing several GCMs. Moghadam et al. (2019) investigated the effect of climate change on runoff of the Khorramabad river basin in Lorestan province. To estimate future temperature and precipitation, HadCM3 and CGCM2 were selected as the best models based on the performance criteria of coefficient of determination (R^2), root mean square error (*RMSE*) and mean absolute error (*MAE*). The results of Atmosphere-Ocean General Circulation Models (AOGCM) showed an increase in temperature and a decrease in rainfall in the future. Then, using the Monte Carlo method, 100 samples of the monthly probabilistic distribution of temperature and rainfall were generated based on weighting. After calibration of the IHACRES model, climatic data from (1) five AOGCM models and (2) the developed Monte Carlo model were applied to the IHACRES model and the river flow was simulated in the future. Kalhori et al. (2022) investigated the uncertainty of Third Assessment Report (TAR) and Fifth Assessment Report (AR5) climate models on runoff in Iran's Khorramabad basin for future periods. Using TAR and AR5 models under different emission scenarios, they predicted future temperature and rainfall with downscaling methods. Results showed decreased runoff in most scenarios, particularly with the IHACRES model, indicating potential challenges for water resource management under climate change. The study underscores the importance of considering model uncertainty in runoff projections for effective planning and adaptation strategies.

In order to accurately model runoff flow in catchments, it is necessary to calibrate the parameters affecting runoff production and evaluate the importance and sensitivity of these parameters. Therefore, in the present study, 22 flow parameters of the SWAT model in the baseline period of 1971–2000 are sensitized using the sensitivity process of the SWAT model using the SUFI2 algorithm in the Sanjabi catchment (located in Kermanshah province). Also, appropriate and accurate input data is needed to increase the modeling's accuracy. It is noteworthy to say that due to the effect of climate change on various climatic parameters and water resources, forecasting future temperature and precipitation and modeling future runoff with a suitable hydrological model for future planning by water resources decision-makers is essential. Also, considering the uncertainties of different climate scenario models can help make future forecasts more accurate. For this purpose, in the present study, the observational data and the NCEP CFSR global database are compared. In addition, future runoff under RCP2.6 and RCP8.5 scenarios, which have the lowest and highest carbon dioxide concentrations by 2100, respectively, in the periods (2040–2069) and (2070–2099) is calculated using the developed Monte Carlo model. It should be considered that, in this paper, for the first time sensitivity analysis of streamflow parameters has been conducted with the SWAT model calibrated by observational data and NCEP CFSR global reanalysis climate datasets and assessment future runoff with the developed Monte Carlo Model at the same time.

In this study, we aim to bridge existing gaps in hydrological research by integrating multiple key components that have been addressed separately in previous studies. Specifically, we conduct a sensitivity analysis of streamflow parameters with the SWAT model, calibrated using observational data and NCEP CFSR global reanalysis climate datasets. Additionally, we assess future runoff using a developed Monte Carlo Model. To the best of our knowledge, this is the first attempt to simultaneously conduct sensitivity analysis and future runoff assessment while integrating these diverse components. By considering the interplay between hydrological modeling, climate change effects, and uncertainty assessment, our study provides valuable insights for informing water resources management decisions in a changing climate.

2 Methodology

The methodology entailed determining the geographical location of the region; identifying climate scenarios and emission scenarios; developing a Monte Carlo model using 9 AOGCM models; downscaling of data from Monte Carlo model using LARS-WG model; analyzing the sensitivity of 22 parameters of SWAT model; comparing observational data and NCEP data; and calculating future runoff under two emission scenarios RCP2.6 and RCP8.5 for two periods

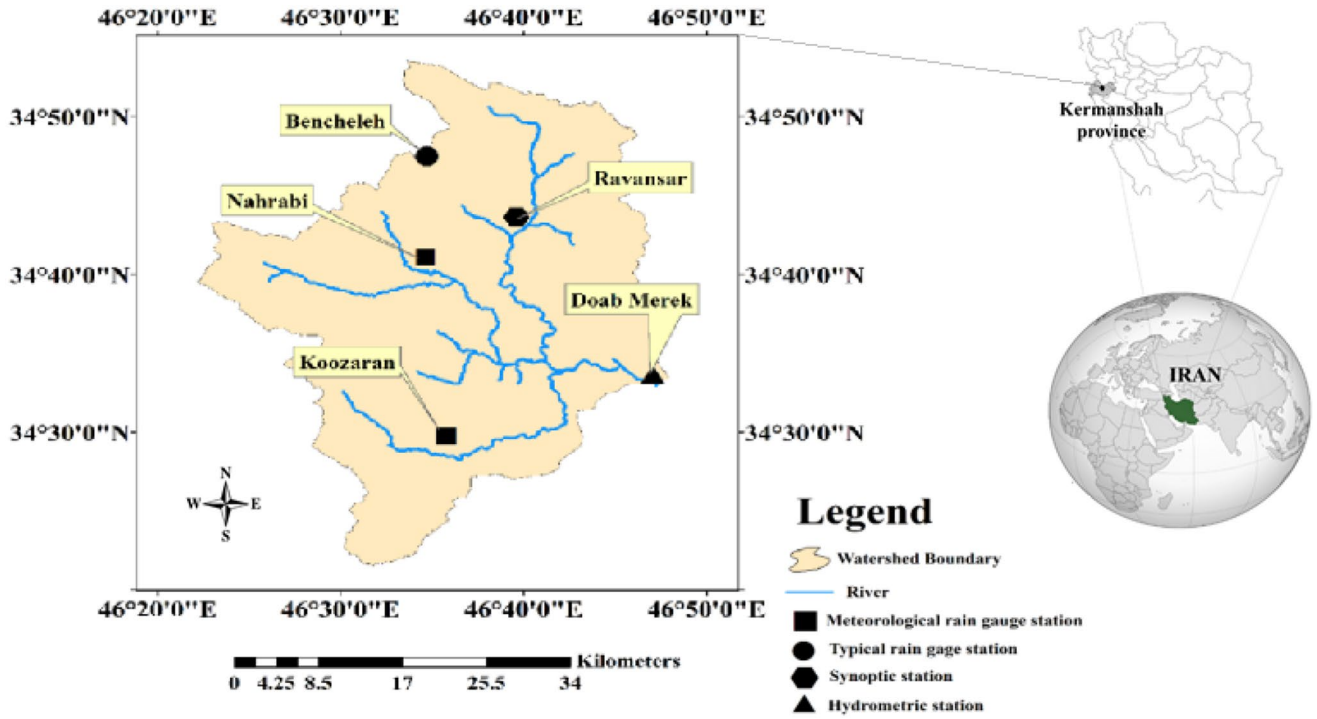

Fig. 1 Location of the study area in Iran and Kermanshah province

Table 1 Specifications of meteorological stations located in the study area

Number	Station name	Elevation (m)	Type of station
1	Doab Merek	1339	Hydrometric
2	Gahvareh	1520	Rain gauge
3	Nahrabi	1490	Rain gauge
4	Ravansar	1363	Synoptic
5	Kermanshah	1318	Rain gauge
6	Javanrood	1375	Rain gauge

2069 – 2040 and 2099 – 2070. Each of these steps is discussed below.

2.1 Location of study area

Sanjabi catchment, with an area of 1230 square kilometers, is one of the Karkheh sub-basins in the northwest of Qarahsu River basin with coordinates of 46 × 40 east longitude and 34 × 33 north latitude in Kermanshah province. The main river in this basin is the Merek River. Figure 1 shows the location of the Sanjabi catchment in Iran and different elevational areas.

Monthly runoff data from Doab Merek and Qarahsu River hydrometric stations as well as rainfall, temperature and other daily meteorological data of selected meteorological and synoptic stations in the basin were collected. The stations used in this study are given in Table 1.

2.2 Future climate scenarios

Future climate scenarios were created with the use of climatic variables simulated by atmospheric-ocean coupled models or global climate models (GCM) (Dubrovsky 1996). These models are based on physical laws expressed by mathematical relationships (Mitchell 2003; Wilby and Harris 2006). In this study, the outputs of nine AOGCM models, including CanESM2, CNRM-CM5, GFDL-CM3, GISS-E2-H, GISS-E2-R, MIROC5, MIROC-ESM, MIROC-ESM-CHEM and MPI-ESM-LR were used.

2.3 Emission scenarios

A non-climatic scenario contains information on the socio-economic status and emissions of greenhouse gases in the Earth's atmosphere, also known as the emission scenario (IPCC-TGCIA 1999). The present study used the fifth assessment report (AR5), which uses RCP scenarios. New emission scenarios are based on the surface forcing radiative by 2100. With the development of greenhouse gas emission scenarios by the intergovernmental panel on climate change (IPCC), atmospheric circulation models with different emission hypotheses have been developed to determine the climatic conditions of the coming decades. In this study, two scenarios, named RCP2.6 and RCP8.5, were used. In RCP2.6, which is the lowest RCP, the total forcing radiative will reach its peak of 3 watts per square meter

by 2050, followed by a decreasing trend, with the lowest concentration of carbon dioxide, and the RCP8.5 scenario is consistently the increase in radiative forcing by the end of the 21st century and is approximately 8.5 watts per square meter, and RCP8.5 has the highest amount of carbon dioxide (Van Vuuren et al. 2011).

2.4 Downscaling

GCM models are currently the only tools that simulate the effects of global climate change on atmospheric elements in large spatial networks. These models simulate atmospheric elements at grids between 150×150 and 250×250 square kilometers (Fung et al. 2011). For this reason, these models cannot consider the effect of local conditions, such as topography, land cover, etc., on atmospheric variables, such as temperature, precipitation, etc. (Prudhomme et al. 2002). Therefore, the LARS-WG model was employed to downscale the data of global climate models to the local scale (Fung et al. 2011). In the present study, for downscaling. The LARS-WG model is a stochastic weather data generator that is used to generate precipitation, radiation, and maximum and minimum daily temperatures at a station under current and future climate conditions.

The first version of the LARS-WG was developed by Rasco et al. (1991) in Budapest, Hungary, as a tool for statistical downscaling. The LARS-WG model uses complex statistical distributions to model meteorological variables, such as the length of dry and wet periods, daily precipitation, and radiation. Rainfall simulation was modeled based on wet and dry days, while wet days are days when rainfall is more than zero millimeter. The length of each series was randomly selected each month. To determine the distributions, the observed data in the previous period were also placed in the same month. To calculate dry days, the amount of rainfall was derived from a semi-experimental distribution of rainfall for a particular month that did not depend on wet series or the amount of rainfall on the previous day (Harmel et al. 2002). Fourier series was used to estimate temperature. The minimum and maximum daily temperatures were modeled as random processes with the mean and deviation of daily criteria that depended on the wet or dry conditions of the day. The third-order Fourier series was used to simulate the mean and standard deviation of the seasonal temperature with a normal distribution. The simulated Fourier series for the mean values was proportional to the mean of observed values. The monitored values for each month had been adjusted to estimate the average daily standard deviation before adjusting the values of the February series deviation.

Simply put, both of these were considered constant for wet and dry values over a year. The residual values obtained by subtracting the mean values from the observed values were used in the temporal autocorrelation analysis of minimum and maximum data. Analysis of the amount of daily radiation in each place showed that the normal distribution of daily radiation in a given climate was inappropriate. The amount of daily radiation on wet and dry days varied significantly.

Therefore, separating the semi-experimental distribution was used to distribute radiation on wet and dry days. Radiation was modeled separately from temperature. Therefore, the inputs of this model were daily climatic statistics, including rainfall, temperature and radiation, and the outputs of this model included minimum temperature, maximum temperature, average monthly and annual temperature, precipitation and radiation values (Semenov and Barrow 2002).

Data production by the model was done in three stages: calibration, evaluation, and creation of meteorological data. The data of the general atmospheric circulation model, including precipitation, minimum temperature, maximum temperature, and radiation, were extracted daily. For each atmospheric global climate model and under each scenario, the LARS-WG model was implemented. To run the LARS-WG model, in addition to the developed scenario for each computing network, there was a need for a file characterizing the past climate behavior of the stations located within that network. According to the model mechanism, first, using the monthly data production scenario, which included the basic climate behavior, all monthly data were calculated according to Eq. (1):

$$F_{fut} = F_{obs} + (F_{GCM}^{fut} - F_{GCM}^{base}) \tag{1}$$

in which F_{fut} = the future data, F_{obs} = the observational data, F_{GCM}^{fut} = the future GCM model data, and F_{GCM}^{base} = the GCM model data in the base state. Then, by keeping the average constant, their standard deviation was changed according to Eq. (2):

$$STD_{fut} = \frac{STD_{obs}}{STD_{base}^{GCM}} \times STD_{fut}^{GCM} \tag{2}$$

2.5 Monte Carlo approach to uncertainty analysis

One of important uncertainties related to climate change is the uncertainty related to different climate models. These models do not get the same results from simulating similar climatic variables in the region due to different methods in downscaling, such as rainfall. Monte Carlo simulation methods are used to analyze the effect of different uncertainties on the system model output. Due to the uncertainty in temperature and rainfall climate change scenarios resulting

from AOGCM models and under different scenarios, runoff from a single temperature and rainfall climate change scenario cannot represent the entire range of runoff. Therefore, it is necessary to select a sample from the unlimited number of climate change scenarios, temperature, and rainfall, and consider the probabilistic distribution for each of the samples and study their effect on the basin runoff.

If the symmetrical distribution is accepted for the temperature and rainfall climate change scenario, the average range of these scenarios will have the most significant impact on runoff. This logic is indicative of the weighting of AOGCM models. In this study, the K-Nearest-Neighbor (KNN) method was used. In this method, AOGCM models were weighted, based on the difference between the mean of climatic variables simulated in the base period from the mean of observed data:

$$W_{m,i} = \frac{\frac{1}{SO_{m,i}}}{\sum_{i=1}^{I} \frac{1}{SO_{m,i}}} \tag{3}$$

in which $SO_{a,i}$ = the difference between the mean of climatic variables (temperature and precipitation) simulated in the baseline period for model i and the long-term mean of month m from the mean of observational data, $W_{m,i}$ = the weight of each model i related to the long-term average of month m, I = the total number of models (in the present study $I = 9$) (Moghadam et al. 2019; Ashofteh et al. 2015).

With the help of SIMLAB software (Giglioli and Saltelli 2003), using the Monte Carlo method and producing 100 samples, the effect of uncertainty of AOGCM models on river runoff was evaluated.

3 Enhanced downscaling methodology

• Downscaling procedure

In this section, we provide a detailed overview of the downscaling methodology employed in our study, focusing on how Monte Carlo samples were utilized as inputs for the LARS-WG model and how the downscaling process was conducted consistently across different GCM models and emission scenarios.

• Generation of Monte Carlo samples

To capture the uncertainty associated with different GCM projections, we employed a Monte Carlo simulation approach. This involved generating 100 samples of probabilistic distributions of basin temperature and rainfall for each GCM model and emission scenario combination. Each Monte Carlo sample represented a plausible climate scenario based on the range of variability among GCM outputs.

• Utilization of Monte Carlo samples in LARS-WG model

The Monte Carlo samples served as inputs for the LARS-WG model, a stochastic weather data generator used for downscaling GCM outputs to the local scale. The LARS-WG model incorporates complex statistical distributions to simulate meteorological variables such as precipitation, radiation, and daily maximum and minimum temperatures under current and future climate conditions.

• Consistent downscaling process

It's essential to note that the downscaling process was conducted consistently across different GCM models and emission scenarios. While the LARS-WG model was implemented separately for each GCM model and emission scenario combination, the methodology for generating Monte Carlo samples remained consistent throughout the analysis. This ensured that the downscaling process adequately represented the uncertainty inherent in GCM projections, regardless of the specific GCM model or emission scenario.

By employing this rigorous downscaling methodology, we aimed to provide robust and reliable projections of future temperature and precipitation at the local scale, facilitating a comprehensive assessment of climate change impacts on surface water resources.

3.1 Rainfall-runoff simulation

In this study, the SWAT model was used to analyze the sensitivity of flow parameters and monthly rainfall-runoff simulation.

• SWAT model

The SWAT model, developed by Arnold et al. (1998), has demonstrated its efficacy in evaluating water resource and nonpoint-source pollution issues across various scales and environmental contexts worldwide.

This model is a physically-based and distributed parameter model developed to predict the effects of land use change, climate change, and management in large and complex catchments (Verbeeten and Barendregt 2007). The model operates at a daily time step and instead of using regression equations to describe the relationship between input and output variables, it provides specific information about air, soil, topography, land use, and land cover in the basin. SWAT is a continuous-time, deterministic, spatially distributed simulator of watershed-scale hydrology. It also provides modules for the simulation of sediment, nutrients, and pesticides in the watershed (Schuo and Abbaspour 2007; Yang et al. 2017).

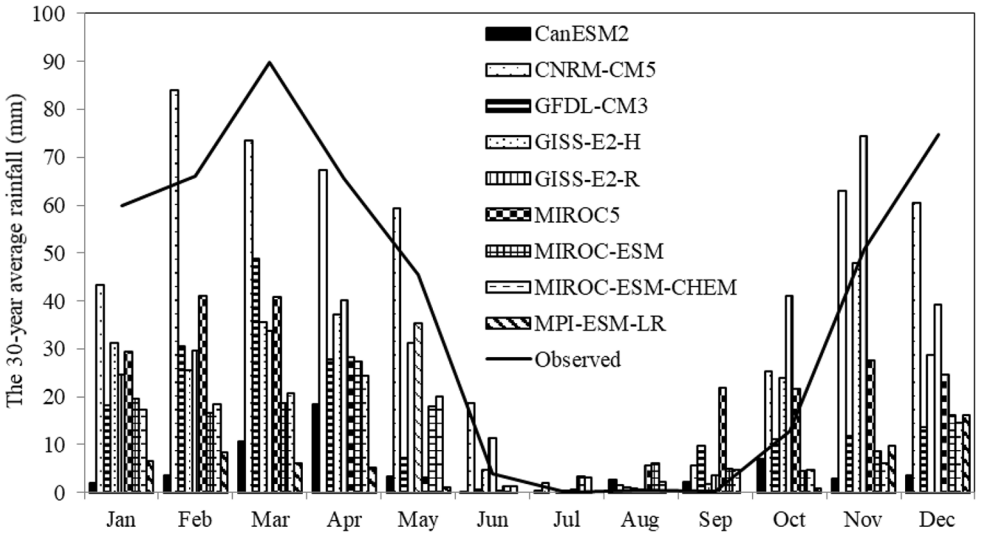

Fig. 2 Comparison of Simulation average monthly precipitation with AOGCM models and observational values in the baseline period 1971–2000

The model divides the basins into sub-basins, each of which is treated as a single unit. Sub-basins are also subdivided into hydrologic response units (HRU), sections of sub-basins with the same digital elevation, land use, and soil properties. It uses the modified curve number method of the U.S. soil conservation service (SCS) or the Green and Ampt infiltration method to calculate surface runoff for each HRU.

The SWAT model provides users with a basin description tool that automatically describes the catchment based on the DEM. It needs to be calibrated and validated for the study area to ensure that its parameters are representative of the study area. The hydrology cycle is simulated using the hydrological balance Eq. (4) (Mengistu 2009):

$$\Delta\, sw = \sum {}^{t}_{i=1}(R_{day} - Q_{surf} - E_a - W_{seep} - Q_{gw}) \qquad (4)$$

in which $\Delta\, sw$ = the change in water stored in the soil, R_{day} = the rainfall, Q_{surf} = the amount of surface runoff, E_a = the real evaporation and transpiration, W_{seep} = the amount of water infiltrated into the unsaturated area of the soil, and Q_{gw} = the amount of groundwater flow (which joins the river, all in millimeters and on a daily time scale).

This model has several parameters due to its complexity, distribution, and the most effective factors in the rainfall-runoff process. Some of the most important parameters required for modeling are: (1) important parameters in simulating the snowmelt process, (2) important parameters in the characteristics of rivers, (3) effective parameters in determining surface runoff, (4) parameters used to define and identify the status of hydrological units, and (5) effective parameters in simulating groundwater flow.

In order to optimize the parameters of the region and determine the range of changes as well as their optimal value and also to analyze the sensitivity of parameters affecting flow, there are different optimization algorithms in SWAT software, such as SUFI2, PSO, GLUE and ParaSol. In the present study, the SUFI2 algorithm was used, one of the most widely used algorithms in SWAT software.

• SUFI2 algorithm

This algorithm defines the difference between observational and simulated data (Rostamian et al. 2008). SWAT-CUP provides the flexibility to employ various algorithms during the calibration or validation process. In this study, the SUFI-2 algorithm (Abbaspour et al. 2004), a semi-automated method utilized for model calibration, validation, sensitivity, and uncertainty analysis, was employed. In the SUFI2 algorithm, measurement of uncertainty in modeling includes uncertainty in inputs, conceptual model, and factors, and is evaluated by the p-factor criterion, which indicates the percentage of measured data that is within the 95% prediction uncertainty (95 PPU). (For a detailed explanation of the SUFI-2 algorithm, including formulas and methodologies, refer to Abbaspour et al. (2004) and Abbaspour et al. (2007).

In the SUFI2 algorithm, it is assumed that each unknown parameter is uniformly distributed over a domain with a certain uncertainty. It should be noted that in both methods, the degree of uncertainty is calculated based on *p-factor* and *r-factor* (Abbaspour et al. 2004, 2007).

The objective function used in SWAT-CUP for model evaluation is the Nash Sutcliffe Efficiency (*NSE*). The *NSE* measures how well the simulated data match the observed data, with values ranging from -∞ to 1, where 1 indicates a perfect match. For further details on *NSE* and its calculation, refer to Nash and Sutcliffe (1970).

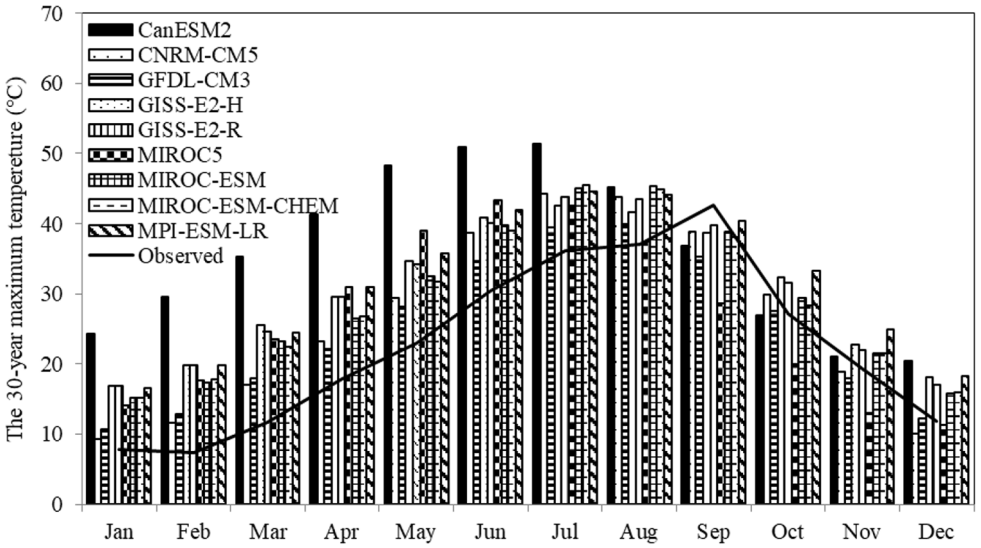

Fig. 3 Comparison of Simulation average monthly maximum temperature with AOGCM models and observational values in the baseline period 1971–2000

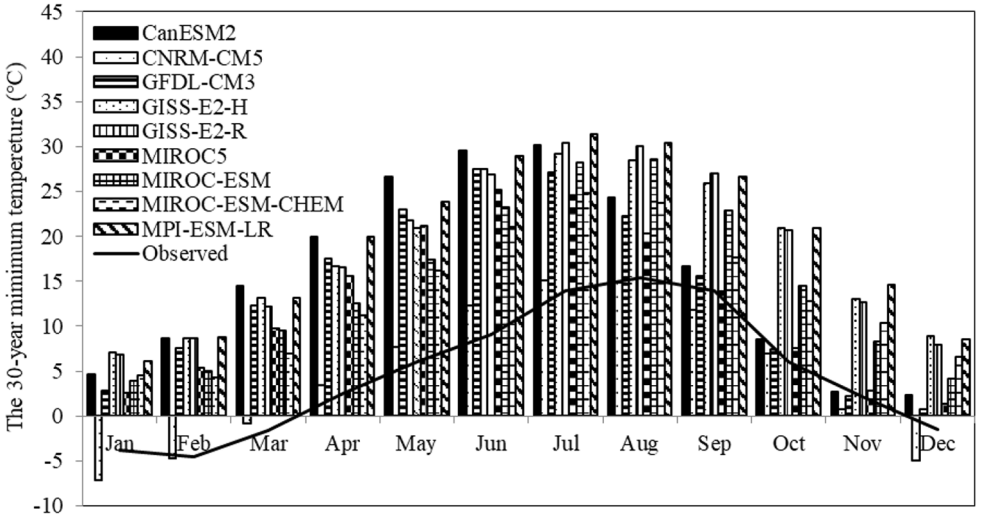

Fig. 4 Comparison of Simulation average monthly minimum temperature with AOGCM models and observational values in the baseline period 1971–2000

4 Results and discussion

4.1 Climatic scenario

First, using the output of 9 AOGCM models related to the fifth IPCC report, including CanESM2, CNRM-CM5, GFDL-CM3, GISS-E2-H, GISS-E2-R, MIROC5, MIROC-ESM, MIROC-ESM-CHEM, and MPI-ESM LR, the modeled values of precipitation, maximum temperature, and minimum temperature were compared with observed values in the baseline period (1971–2000) and results are presented in Figs. 2, 3 and 4. According to Fig. 2, it can be seen that all models from late summer to early summer had modeled less rainfall than the observed values, and only in February and May, more rainfall than the observed values was reported by the CNRM-CM5 model. Comparing the models, it can be seen that the CNRM-CM5 model had the highest and the CanESM2 and MPI-ESM-LR models had the lowest rainfall in most months. According to Fig. 3, it can be seen that in winter, spring and late autumn, all models simulated higher maximum temperatures than the observed values, and from September to December, some models simulated maximum temperatures lower than observed values. It can also be seen that the CanESM2 model had simulated the maximum temperature in winter, spring and early summer with a large difference compared to other models, but this difference was not seen in other months. According to Fig. 4, it can be seen that all models simulated higher minimum temperatures than the observed values in all seasons of the year, and only in January and December, the CNRM-CM5 model had modeled the minimum temperature below the observed values. It is also noteworthy that in the winter and spring seasons, the CanESM2 model and in the other two seasons (summer and autumn), the MPI-ESM-LR model simulated the minimum temperature more than all the models.

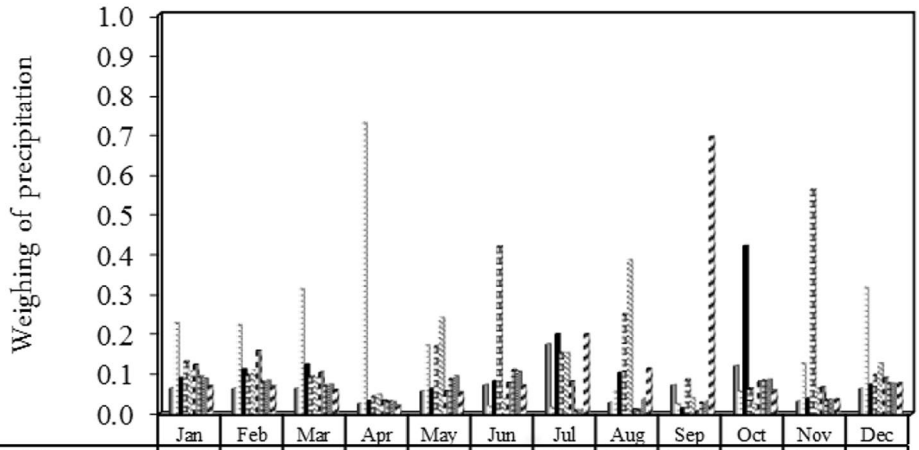

	Jan	Feb	Mar	Apr	May	Jun	Jul	Aug	Sep	Oct	Nov	Dec
CanESM2	0.065	0.064	0.065	0.027	0.058	0.073	0.175	0.029	0.073	0.121	0.032	0.064
CNRM-CM5	0.228	0.223	0.313	0.728	0.173	0.019	0.016	0.056	0.025	0.057	0.126	0.316
GFDL-CM3	0.091	0.112	0.125	0.033	0.063	0.083	0.200	0.103	0.015	0.421	0.039	0.074
GISS-E2-H	0.132	0.098	0.094	0.044	0.170	0.420	0.154	0.250	0.086	0.065	0.562	0.098
GISS-E2-R	0.107	0.110	0.091	0.049	0.242	0.039	0.154	0.386	0.041	0.025	0.065	0.127
MIROC5	0.124	0.159	0.104	0.034	0.057	0.079	0.082	0.012	0.006	0.081	0.067	0.090
MIROC-ESM	0.094	0.081	0.072	0.033	0.088	0.110	0.009	0.011	0.029	0.085	0.036	0.077
MIROC-ESM-CHEM	0.089	0.084	0.074	0.031	0.095	0.106	0.010	0.038	0.031	0.087	0.034	0.075
MPI-ESM-LR	0.071	0.069	0.061	0.021	0.055	0.072	0.200	0.114	0.695	0.059	0.038	0.077

Fig. 5 Models weighing of precipitation

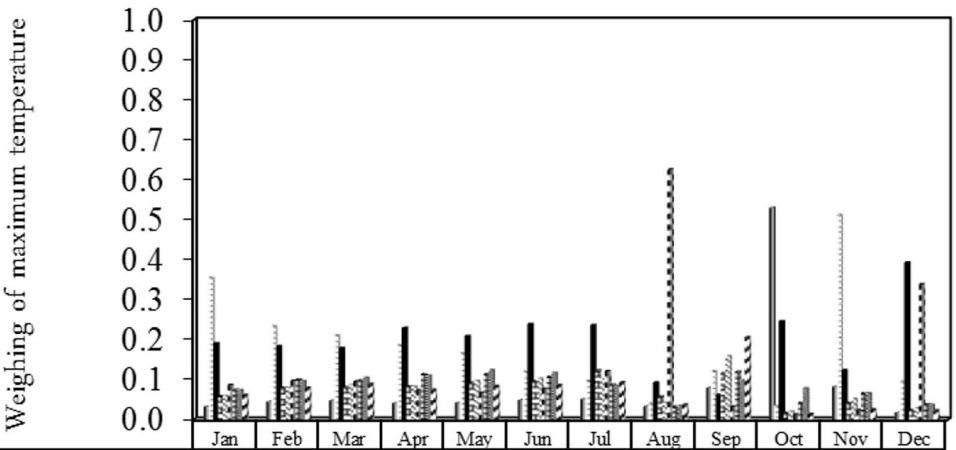

	Jan	Feb	Mar	Apr	May	Jun	Jul	Aug	Sep	Oct	Nov	Dec
CanESM2	0.033	0.045	0.048	0.042	0.043	0.049	0.052	0.034	0.080	0.530	0.083	0.018
CNRM-CM5	0.355	0.234	0.211	0.186	0.167	0.121	0.097	0.040	0.122	0.034	0.512	0.095
GFDL-CM3	0.191	0.184	0.180	0.230	0.209	0.239	0.237	0.093	0.063	0.247	0.125	0.393
GISS-E2-H	0.060	0.080	0.082	0.084	0.093	0.097	0.123	0.058	0.117	0.018	0.042	0.024
GISS-E2-R	0.061	0.080	0.089	0.084	0.097	0.104	0.102	0.042	0.160	0.021	0.053	0.030
MIROC5	0.087	0.097	0.096	0.075	0.068	0.078	0.122	0.626	0.033	0.013	0.024	0.339
MIROC-ESM	0.075	0.101	0.099	0.114	0.114	0.108	0.088	0.033	0.120	0.043	0.067	0.039
MIROC-ESM-CHEM	0.075	0.097	0.106	0.110	0.124	0.118	0.084	0.035	0.099	0.079	0.067	0.038
MPI-ESM-LR	0.063	0.081	0.090	0.075	0.085	0.087	0.094	0.038	0.207	0.015	0.026	0.024

Fig. 6 Models weighing of maximum temperature

4.2 Monte Carlo simulation

To use the SIMLAB model and calculate the uncertainty using the Monte Carlo method, it was necessary to specify the temperature and rainfall climate change scenarios for the nine AOGCM models under two scenarios: RCP2.6 and RCP8.5 and two periods 2040–2069 and 2070–2099, as well as the weight of each model for each month (long-term average) relative to the observed values. The weighted

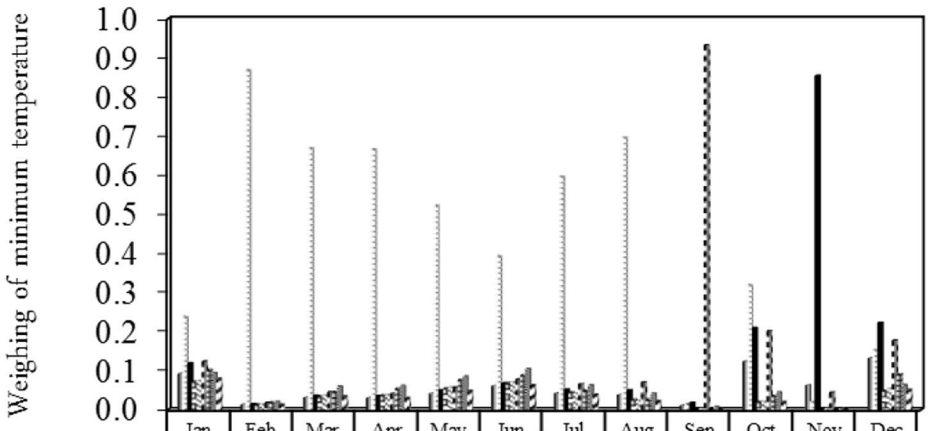

	Jan	Feb	Mar	Apr	May	Jun	Jul	Aug	Sep	Oct	Nov	Dec
CanESM2	0.093	0.014	0.032	0.031	0.042	0.062	0.043	0.039	0.012	0.124	0.063	0.133
CNRM-CM5	0.238	0.869	0.669	0.666	0.523	0.393	0.597	0.697	0.016	0.319	0.021	0.153
GFDL-CM3	0.120	0.015	0.037	0.036	0.051	0.069	0.053	0.051	0.019	0.211	0.855	0.223
GISS-E2-H	0.073	0.014	0.035	0.038	0.056	0.069	0.046	0.027	0.003	0.021	0.003	0.050
GISS-E2-R	0.075	0.014	0.038	0.039	0.059	0.071	0.042	0.024	0.003	0.021	0.003	0.055
MIROC5	0.124	0.019	0.046	0.042	0.058	0.078	0.066	0.071	0.933	0.202	0.045	0.178
MIROC-ESM	0.103	0.020	0.047	0.054	0.077	0.089	0.049	0.026	0.004	0.036	0.005	0.092
MIROC-ESM-CHEM	0.095	0.021	0.060	0.062	0.086	0.106	0.064	0.042	0.009	0.046	0.004	0.064
MPI-ESM-LR	0.080	0.014	0.035	0.031	0.049	0.063	0.040	0.023	0.003	0.021	0.002	0.052

Fig. 7 Models weighing of minimum temperature

values for precipitation, maximum temperature, and minimum temperature are presented in Figs. 5, 6 and 7.

The higher the weight of the model, the greater is the effect of that model on the climatic parameter (temperature or rainfall). According to Figs. 5, 6 and 7, it can be seen that CNRM-CM5 and MIROC-ESM models had the highest and lowest weights for precipitation, respectively. For maximum temperature, these values we are for GFDL-CM3 and GISS-E2-H models, respectively. Regarding the minimum temperature, the CNRM-CM5 model had the most effect and the MPI-ESM-LR model had the least effect.

After weighting the models, the monthly probabilistic distribution functions of temperature and rainfall climate change scenarios were calculated. Finally, using the Monte Carlo simulation method and SIMLAB software, 100 samples of temperature and rainfall climate change scenarios were extracted from each probabilistic scattering function. Subsequently, 100 monthly time series of temperature and rainfall were produced.

4.3 Calculation of climate change scenarios in future periods

After calculating the temperature and rainfall climate change scenarios by Monte Carlo model, the LARS-WG model was used for downscaling and calculating future temperature and precipitation under two scenarios of RCP2.6 and RCP8.5 and the future periods 2040–2069 and 2070–2099. The amounts of calculated values relative to the observed

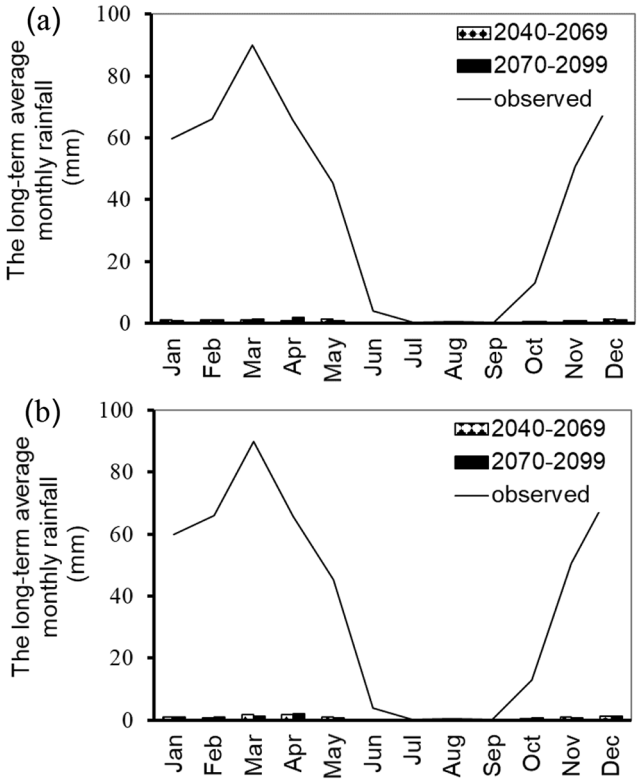

Fig. 8 Average monthly precipitation in the next two periods (2040–2069) and (2070–2099) for scenario (**a**) RCP2.6, (**b**) RCP8.5

values are shown in Figs. 8 and 9, and 10. As shown in Figs. 8 and 9, and 10, future precipitation in both scenarios RCP2.6 and RCP8.5 and in the future periods 2040–2069

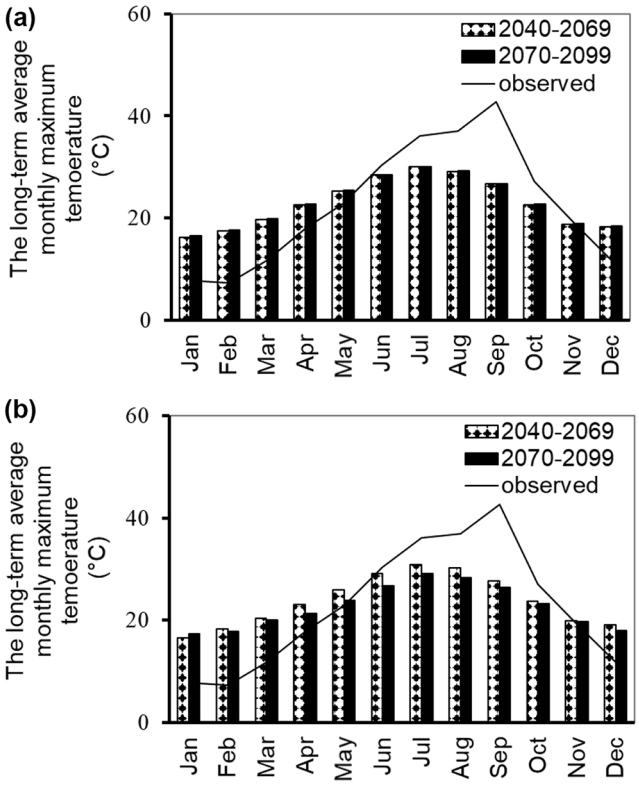

Fig. 9 Average monthly maximum temperature in the next two periods (2040–2069) and (2070–2099) for scenario (**a**) RCP2.6, (**b**) RCP8.5

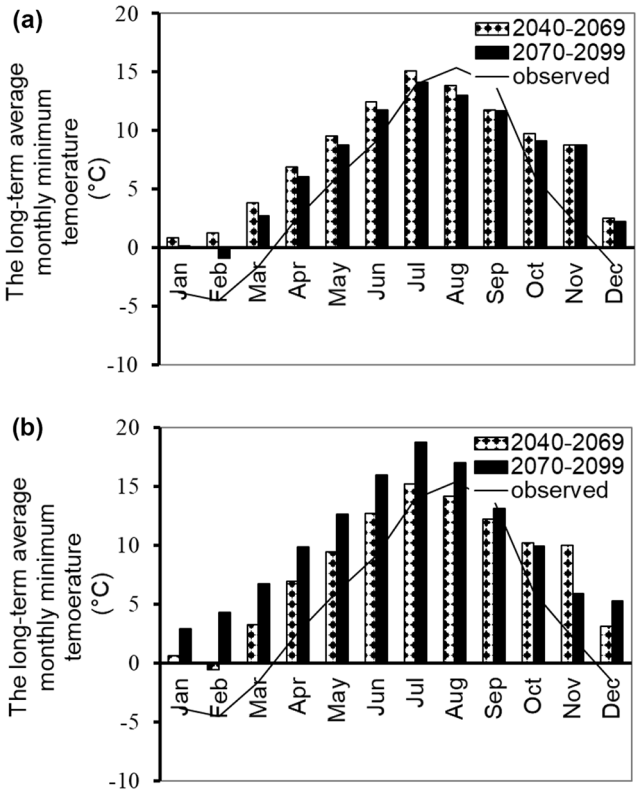

Fig. 10 The average monthly minimum temperature in the next two periods (2040–2069) and (2070–2099) for scenario (**a**) RCP2.6, (**b**) RCP8.5

and 2070–2099 would be significantly reduced compared to the observed values in all months. Regarding the maximum temperature, it was observed in both scenarios RCP2.6 and RCP8.5 and in the future periods 2040–2069 and 2070–2099 from late autumn to late spring, the maximum temperature would increase compared to the observed values and this rate would decrease in summer. Regarding the minimum temperature, it can be said that in both future periods and in both RCP2.6 and RCP8.5 scenarios, there will be an increase in the minimum temperature in all months except August and September.

4.4 Calibration and validation results for SWAT models

Information about each of the soils and land uses in the Sanjabi basin was manually entered into the SWAT model database. By combining three digital elevation maps (DEM), soil and land use together and slope classification into five floors, HRUs were determined in the study basin. Slope classification was done in five categories: 0-10.66, 10.66–21.33, 21.33–31.99, 31.99–42.66 and 42.66–53.33 degrees.

In the SWAT model, 33 sub-basins and 260 HRUs were delineated in the Sanjabi basin. Then, daily rainfall and the maximum and minimum daily temperatures of stations near the basin in the 30-year period 1971–2000 were entered into the model. After introducing the required information, considering the monthly scale of 1971, 1972, and 1973 as Warm-Up, the SWAT2012 model was implemented in ArcGIS10.2 software with a monthly time step. Given that the initial values of some basin properties, such as soil chemical composition, may not be available, the SWAT model in the Warm-Up period can stabilize or calculate these values.

After each run of the SWAT model, for each simulation, outputs, including runoff components, subsurface flow, groundwater storage, etc., were obtained as a text file containing information. This text file was stored in folders called TxtIntOut. By connecting this folder to the SWAT-CUP software and selecting the algorithm (in this research, SUFI2 algorithm), 22 effective parameters in the flow in the statistical period of 1974–1991 were calibrated. The validation period was 1992–2000.

The SWAT model was calibrated once with observational data and once with NCEP CFSR global database. The validation and calibration results of the SWAT model with both observational data and NCEP CFSR global database are shown in Tables 2 and 3 and the river flow time series for the calibration and validation periods are shown in Figs. 11 and 12, respectively. The higher the R^2 and the lower the

Table 2 SWAT model performance criteria with observational data

Time period	R^2 (%)	RMSE (m^3/s)	MAE (m^3/s)	NSE (Dimensionless)	PBIAS (%)
1974–1991 (Calibration)	63	57	3	0.6	0.05
1992–2000 (Verification)	57	5	3	0.5	0.09

Table 3 SWAT model performance criteria with NCEP CFSR global database

Time period	R^2 (%)	RMSE (m^3/s)	MAE (m^3/s)	NSE (Dimensionless)	PBIAS (%)
1974–1991 (Calibration)	29	12	9	-0.9	-1.04
1992–2000 (Verification)	25	16	8	-3.9	-0.99

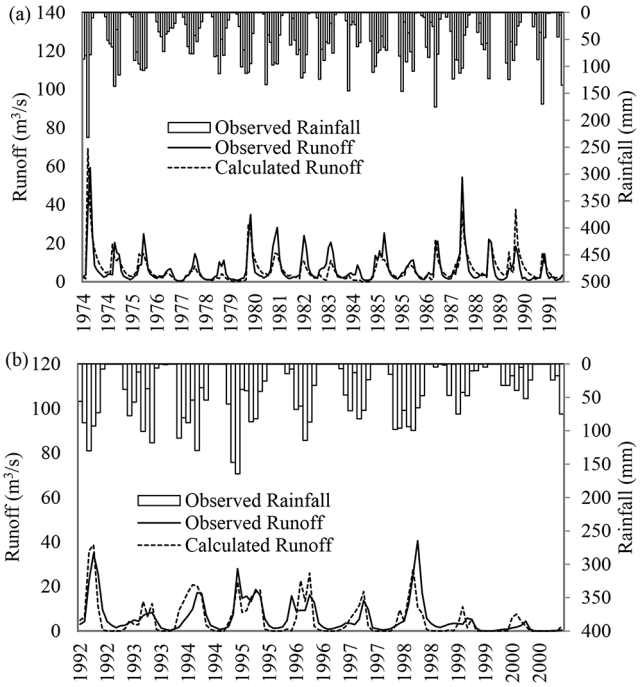

Fig. 11 Comparison of simulated and observed runoff by SWAT model with observational data in the period (**a**) calibration (1974–1991) and (**b**) verification (1992–2000)

error, the better was the model performance. PBIAS (Percent Bias) was calculated to assess the average tendency of the modeled data compared to the observed data. A positive PBIAS indicates an overestimation, while a negative PBIAS indicates an underestimation of the modeled runoff. According to the calibration results of the SWAT model with both observational data and the NCEP CFSR global database, it can be seen that in general, the efficiency of the SWAT model with the observational data had a good performance, but the performance of the SWAT model with the NCEP CFSR global database was not satisfactory. The parameters used in the calibration and the optimal values

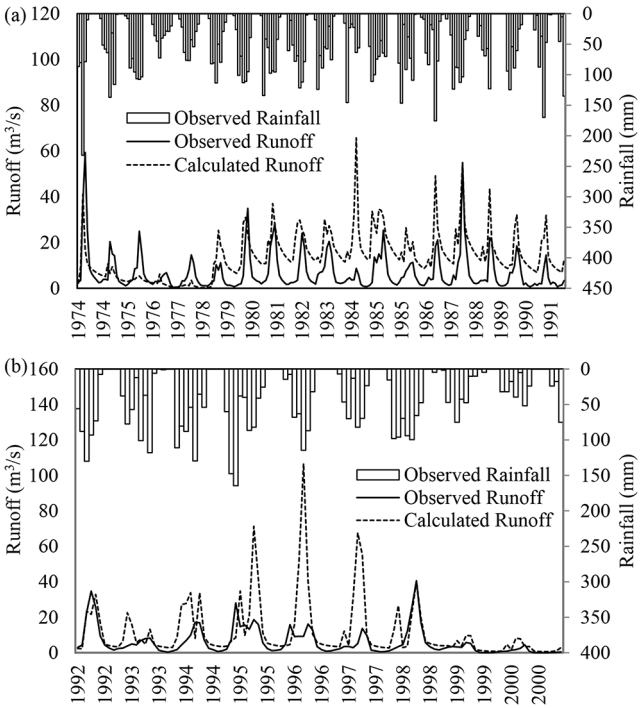

Fig. 12 Comparison of simulated and observed runoff by SWAT model with NCEP CFSR global database in the period (**a**) calibration (1974–1991) and (**b**) verification (1992–2000)

of these parameters are given in Table 4 which shows the range of variations as well as the optimal values for the various parameters affecting the region. In fact, the optimal value of each parameter was only based on the improvement of the objective function, and the changes of different parameters were separate from each other and had no effect on each other. In other words, to determine the sensitivity of each parameter, by changing its value and keeping the values of other parameters constant, the objective functions was examined and this process was repeated for all parameters. Finally, the parameters which had the greatest effect on the objective function were identified as the most sensitive parameters.

To analyze the sensitivity of parameters affecting flow, two parameters t-Stat and P-Value were used. Thus, the lower the P-value and the higher the t-Stat value, the greater the parameter's effect on flow. In Table 5; Fig. 13, the desired parameters (their effect from lowest to highest, respectively) are given with the t-Stat and P-Value values.

According to Table 5; Fig. 13, it was observed that the parameters CN2 (initial SCS curve number for medium humidity conditions) and SFTMP (snowfall temperature (degrees Celsius)) which had the highest t-Stat value and the lowest P-value, were the most effective parameters. RCHRG_DP (shallow to deep aquifer transfer coefficient) and PLAPS (temperature elevation gradient) parameters,

Table 4 Parameters used in the calibration stage and the optimal values of these parameters

Number	Parameter name	Parameter abbreviation	Parameter range	Optimal value
1	SCS runoff curve number for moisture condition	CN2	-0.2–0.2	-0.19
2	Base flow alpha factor (days)	ALPHA_BF	0.46–1	0.69
3	Groundwater delay time (days)	GW_DELAY	30–254.11	111.9
4	Threshold depth of water in the shallow aquifer required for return flow to occur	GWQMN	0.62–1.88	1.54
5	Soil evaporation compensation factor	ESCO	0.19–0.73	0.11
6	Effective hydraulic conductivity in main channel alluvium (mm/hr)	CH_K2	14.31–104.79	141.25
7	Manning roughness for main channel	CH_N2	0.1–0.3	0.24
8	Base flow alpha factor for bank storage (days)	ALPHA_BNK	0–0.6	0.79
9	Groundwater revap coefficient	GW_REVAP	0–0.11	0.09
10	Deep aquifer percolation fraction	RCHRG_DP	0.41–1	0.54
11	Soil bulk density	SOL_BD	0.82–2.5	1.02
12	Soil available water capacity (mm)	SOL_AWC	-0.2–0.16	0.28
13	Soil hydraulic conductivity (mm/hr)	SOL_K	0–0.58	0.52
14	overland manning roughness	OV_N	0.16–0.59	0.35
15	Threshold depth of water in the shallow aquifer for ‘revap’ to occur (mm)	REVAPMN	0–500	3.92
16	Surface runoff lag coefficient (days)	SURLAG	8.47–25.31	20.05
17	Snowfall temperature (°C)	SFTMP	0.82–2.5	4.25
18	Snowmelt base temperature	SMTMP	-0.2–0.16	17.21
19	Temperature lapse rate(°C/km)	TLAPS	0–0.58	32.92
20	Precipitation altitude gradient (mm H_2O/km)	PLAPS	0.16–0.59	20.5
21	plant uptake compensation factor	EPCO	0–500	0.47
22	Maximum canopy storage	CANMX	8.47–25.31	94.17

Table 5 The results of SUFI2 algorithm (t-stat, P-value)

Number	Parameter name	Parameter abbreviation	t-Stat	*P*-Value
1	Deep aquifer percolation fraction	RCHRG_DP	0.06	0.96
2	Precipitation altitude gradient (mm H_2O/km)	PLAPS	0.24	0.81
3	Temperature lapse rate(°C/km)	TLAPS	0.31	0.76
4	Threshold depth of water in the shallow aquifer for ‘revap’ to occur (mm)	REVAPMN	0.37	0.72
5	Threshold depth of water in the shallow aquifer required for return flow to occur	GWQMN	0.4	0.69
6	Soil evaporation compensation factor	ESCO	0.41	0.68
7	Soil hydraulic conductivity (mm/hr)	SOL_K	0.57	0.57
8	Soil available water capacity (mm)	SOL_AWC	0.62	0.53
9	overland manning roughness	OV_N	0.91	0.37
10	plant uptake compensation factor	EPCO	0.95	0.34
11	Snowmelt base temperature	SMTMP	0.98	0.33
12	Soil bulk density	SOL_BD	1.05	0.29
13	Base flow alpha factor for bank storage (days)	ALPHA_BNK	1.12	0.27
14	Maximum canopy storage	CANMX	1.2	0.23
15	Surface runoff lag coefficient (days)	SURLAG	1.4	0.16
16	Manning roughness for main channel	CH_N2	1.5	0.13
17	Effective hydraulic conductivity in main channel alluvium, mm/hr	CH_K2	1.52	0.13
18	Groundwater revap coefficient	GW_REVAP	1.62	0.11
19	Base flow alpha factor (days)	ALPHA_BF	1.8	0.07
20	Groundwater delay time (days)	GW_DELAY	2.71	0.01
21	Snowfall temperature (°C)	SFTMP	3.65	0.00
22	SCS runoff curve number for moisture condition	CN2	30.62	0.00

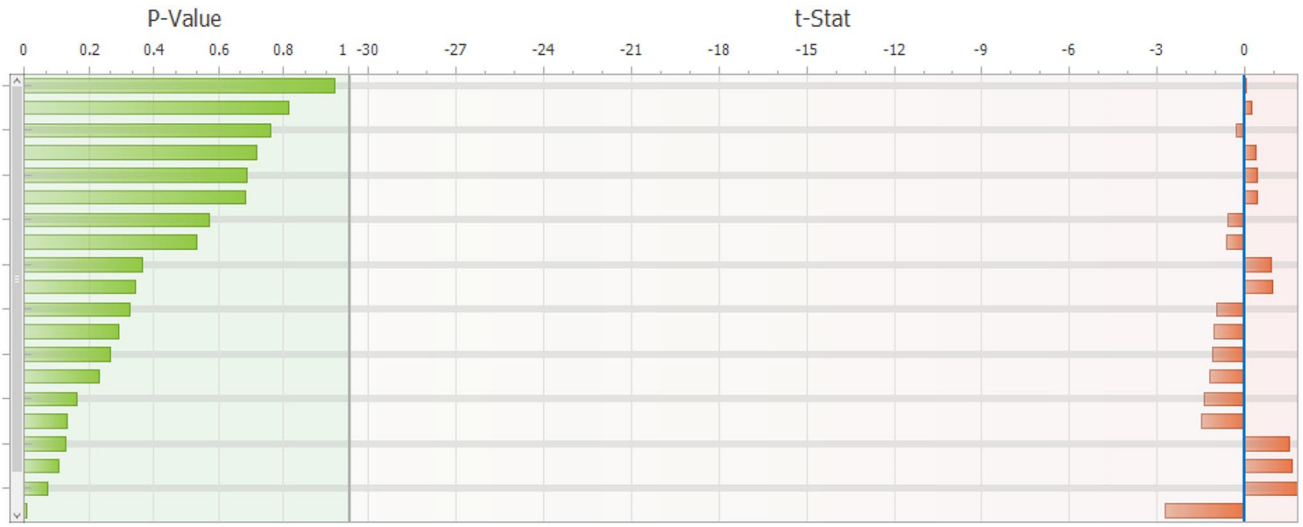

Fig. 13 Sensitivity of parameters in SUFI2 algorithm (t-stat, P-value)

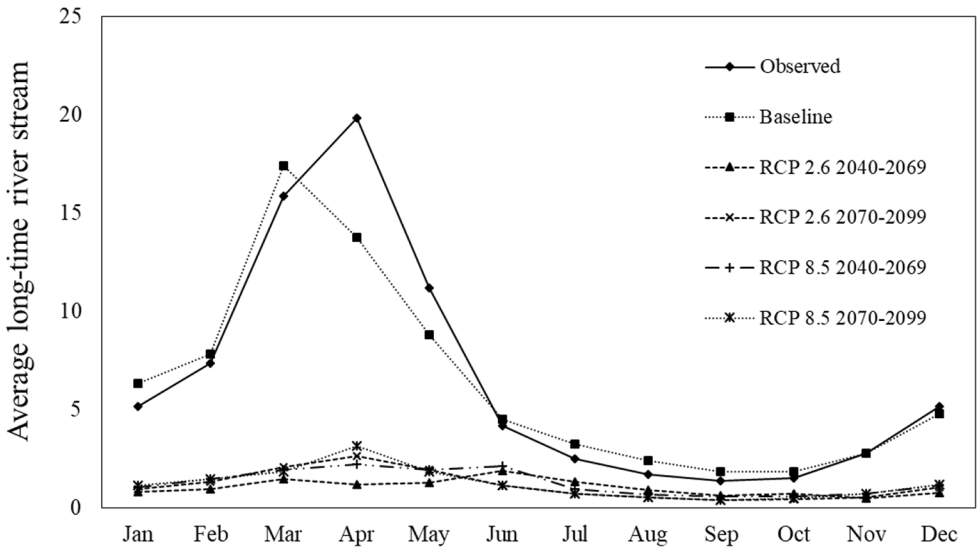

Fig. 14 Comparison of monthly long-term river flow (runoff) in the period 2040–2069 and 2070–2099 for RCP2.6 and RCP8.5 Scenarios with baseline and observation values

which had the lowest t-Stat value and the highest P-value, had the least impact on flow.

4.5 Simulation of river flow in future periods

Using the SWAT model, the monthly time series of river flow was simulated using future estimated temperature and precipitation data using the LARS-WG model. Figure 14 shows a comparison of the average long-term monthly river flow in the future periods 2040–2069 and 2070–2099 for RCP2.6 and RCP8.5 scenarios with baseline and observational values. Also, the values of average long-term runoff of observational, baseline, and simulated runoff in future periods and different scenarios are given in Table 6. According to Fig. 14; Table 6, it can be seen that the simulated runoff values will decrease in the future periods in both scenarios compared to the simulated baseline values in all months, while this decrease in winter and spring seasons is much longer than the summer and autumn seasons and peaks in March. This trend is also true for comparing future runoff with observational values. With the difference that only in April will there be the maximum reduction. Comparing the scenarios with each other, it should be said that in general, RCP2.6 scenario in the future periods will show more runoff reduction in the future than RCP8.5 scenario. The reason for this can be the constant trend of changes in radiative forcing until 2100 in RCP8.5, while changes in radiative forcing for RCP2.6 are variable and will increase and then decrease until 2050.

The annual changes in runoff simulated with the SWAT model relative to the observed values are given in Table 7. As shown in Table 7, the annual runoff reduction under the RCP2.6 scenario for the future periods 2040–2069 and 2070–2099 is 84.09% and 82.45%, respectively, and

Table 6 The average long-term observation, base and future runoff in 2040–2069 and 2070–2099 periods in RCP2.6 and RCP8.5 scenarios (m^3/s)

Month	Observation	Baseline	RCP2.6		RCP8.5	
			2040–2069	2070–2099	2040–2069	2070–2099
Jan	5.16	6.33	0.81	0.97	1.04	1.16
Feb	7.36	7.84	0.96	1.35	1.45	1.47
Mar	15.86	17.37	1.47	2.09	1.93	1.84
Apr	19.81	13.77	1.21	2.62	2.23	3.13
May	11.19	8.78	1.27	1.94	1.94	1.84
Jun	4.20	4.53	1.9	1.16	2.14	1.13
Jul	2.51	3.23	1.32	0.74	0.96	0.74
Aug	1.72	2.4	0.92	0.52	0.7	0.53
Sep	1.37	1.85	0.65	0.4	0.59	0.41
Oct	1.5	1.83	0.73	0.42	0.56	0.49
Nov	2.77	2.79	0.48	0.55	0.73	0.72
Dec	5.17	4.79	0.78	1.04	1.16	1.17

Table 7 The annual changes in simulation runoff relative to the observed values (%)

Percentage of runoff changes			
RCP2.6		RCP8.5	
2040–2069	2070–2099	2040–2069	2070–2099
-84	-82	-80	-81

the RCP8.5 scenario for the period 2040–2069, decreases by 80.38% and for the period 2070–2099, it decreases by 81.39%, which is very significant.

5 Conclusion

The present study investigates the effect of climate change on surface water resources and analyzes the sensitivity of flow parameters of the Sanjabi basin in Kermanshah province in Iran. For this purpose, the output of nine AOGCM models, including CanESM2, CNRM-CM5, GFDL-CM3, GISS-E2-H, GISS-E2-R, MIROC5, MIROC-ESM, MIROC-ESM-CHEM and MPI-ESM-LR were used. After determining the range of climate change scenarios, each model was weighted. Then, based on weighting, using the Monte Carlo method, 100 samples of the basin's monthly probabilistic distribution functions of temperature and rainfall were generated. The LARS-WG model was used for downscaling and then temperature and future precipitation for the periods 2040–2069 and 2070–2099 were calculated under the RCP2.6 and RCP8.5 scenarios.

The SWAT model was then used to simulate surface runoff. For the SWAT model, two observational data and the NCEP CFSR global database were compared. Both models were calibrated and their efficiency was measured. With observational data, the model had coefficients of R^2, *RMSE*, *MAE* and *NSE* in the amount of 63.04%, 5.18 m^3/s, 3.17 m^3/s and 0.61 in the calibration period (1971–1990) and 56.85%, 5.52 m^3/s, 3.49 m^3/s and 0.47 in the validation period (1992–2002) had better performance and therefore this model was used to predict future runoff. By comparing monthly long-term runoff under the RCP2.6 and RCP8.5 scenarios in the periods 2040–2069 and 2070–2099 with the baseline values, it was found that in all scenarios and future periods, the amount of runoff decreased significantly. Also, the annual runoff rate will decrease by 84.09%, 82.45, 80.38 and 81.39%, respectively, compared to the observations for the RCP2.6 and RCP8.5 scenarios for the future periods 2040–2069 and 2070–2099.

Author contributions Seyedeh Hadis Moghadam developed the theory and performed the computations. Parisa-Sadat Ashofteh verified the analytical methods and encouraged Seyedeh Hadis Moghadam to investigate a specific aspect. Parisa-Sadat Ashofteh supervised the findings of this work, and Vijay P. Singh helped supervise the project. All authors discussed the results and contributed to the final manuscript. Seyedeh Hadis Moghadam wrote the manuscript with support from Parisa-Sadat Ashofteh, especially Vijay P. Singh. Parisa-Sadat Ashofteh conceived the original idea.

Funding Not applicable.

Data availability Those will be made available on reasonable request.

Declarations

Ethical approval The paper is not currently being considered for publication elsewhere. All authors have been personally and actively involved in substantial work leading to the paper, and will take public responsibility for its content.

Consent to participate Informed consent was obtained from all individual participants included in the study.

Consent to publish The participant has consented to the submission of the case report to the journal.

Competing interests The authors declare no competing interests.

References

Abbaspour KC, Johnson CA, van Genuchten MT (2004) Estimating uncertain flow and transport parameters using a sequential uncertainty fitting procedure. Vadose Zone J 3(4):1340–1352. https://doi.org/10.2113/3.4.1340

Abbaspour KC, Yang J, Maximov I, Siber R, Bogner K, Mieleitner J, Zobrist J, Srinivasan R (2007) Modelling of hydrology and water quality in the pre-alpine/alpine thur watershed using SWAT. J Hydrol 333:413–430. https://doi.org/10.1016/j.jhydrol.2006.09.014

Arnold JG, Srinivasan R, Muttiah RS, Williams JR (1998) Large-area hydrologic modeling and assessment: Part I. Model development. J Am Water Resources Association 34(1):73-89. https://doi.org/10.1111/j.1752-1688.1998.tb05961.x

Ashofteh P-S, Bozorg-Haddad O, Mariño MA (2015) Risk analysis of water demand for agricultural crops under climate change. J Hydrol Eng 20(4). https://doi.org/10.1061/(ASCE)HE.1943-5584.0001053

Dile YT, Srinivasan R (2014) Evaluation of CGSR climate data for hydrologic prediction in data-scarce watersheds: an application in the Blue Nile river basin. J Am Water Resour Assoc 50(5):1226–1241. https://doi.org/10.1111/jawr.12182

Dubrovsky M (1996) Met&Roll: the stochastic generator of daily weather series for the crop growth model. Meteorological Bull 49:97–105 (in Czech)

Fuka DR, Walter MT, MacAlister C, Degaetano AT, Steenhuis TS, Easton ZM (2014) Using the climate forecast system reanalysis as weather input data for watershed models. Hydrol Processes 28(22):5613–5623. https://doi.org/10.1002/hyp.10073

Fung F, Lopez AL, New M (2011) Modeling the impact of climate change on water resources. Wiley-Blackwell, London, ISBN: 978-1-405-19671-0

Ghavidelfar S, Alvankar R, Razmkhah A (2011) A comparison of the lumped and quasi-distributed Clark runoff models in simulating flood hydrographs on a semi-aridwatershed. Water Resour Manag 25:1775–1790. https://doi.org/10.1007/s11269-011-9774-5

Giglioli N, Saltelli A (2003) Simlab 2.2, software for sensitivity and uncertainty analysis. Simlab Manual, Joint Research Centre European Commission

Harmel RD, Richardson CW, Hanson CL, Johnson GL (2002) Evaluating the adequecy of simulating maximum and minimum daily air temperature with the normal distributian. J Appl Meteorol Climatology 41(7):744–753. https://doi.org/10.1175/1520-0450(2002)041%3C0744:ETAOSM%3E2.0.CO;2

IPCC-TGCIA (1999). Guidelines on the use of scenario data for climate impact and adaptation assessment. In: Carter TR, Hulme M, Lal M (eds.) Intergovernmental panel on climate change, task group on scenarios for climate impact assessment, Version 1, 69 pp

Kalhori M, Ashofteh P-S, Moghadam SH, Singh VP (2022) Investigating the effect of uncertainty of AOGCM-TAR and AOGCM-AR5 climate change models on river runoff. Arab J Geosci 15. https://doi.org/10.1007/s12517-022-10471-1

Kalhori M, Ashofteh P-S, Moghadam SH (2023) Development of the multi-objective invasive weed optimization algorithm in the integrated water resources allocation problem. Water Resour Manage 37:4433–4458. https://doi.org/10.1007/s11269-023-03564-3

Kim J, Choi J, Choi C, Park S (2013) Impacts of changes in climate and land use/land cover under IPCC RCP scenarios on streamflow in the Hoeya River Basin, Korea. Sci Total Environ 452–453. https://doi.org/10.1016/j.scitotenv.2013.02.005

Li ZJ, Zhang K (2008) Comparison of three GIS based hydrological models. J Hydrologic Eng 13(5). https://doi.org/10.1061/(ASCE)1084-0699(2008)13:5(364)

Mengistu KT (2009) Watershed hydrological responses to changes in land use and land cover, and management practises at Hare Watershed, Ethiopia, Thesis, Siegen University, Fakultät Bauingenieurwesen Research Institute for water and Environment, 229 pages

Mishra A, Froebrich J, Gassman PW (2007) Evaluation of the SWAT model for assessing sediment control structures in a small watershed in India. Trans ASABE (American Soc Agricultural Biol Engineers) 50(2):469–477. https://doi.org/10.13031/2013.22637

Mitchell TD (2003) Pattern scaling: an examination of the accuracy of the technique for describing future climates. Clim Change 60(3):217–242

Moghadam SH, Ashofteh P-S, Loáiciga HA (2019) Application of climate projections and Monte Carlo approach for the assessment of future river flow: case study of the Khorramabad River basin, Iran. J Hydrol Eng 24(7). https://doi.org/10.1061/(ASCE)HE.1943-5584.0001801

Moghadam SH, Ashofteh P-S, Loáiciga HA (2023a) Use of surface water and groundwater under climate change: Khorramabad basin, Iran. In: Proceedings of the Institution of Civil Engineers - Water Management, 53–65, https://doi.org/10.1680/jwama.19.00011

Moghadam SH, Ashofteh P-S, Loáiciga HA (2023b) Investigating the performance of data mining, lumped, and distributed models in runoff projected under climate change. J Hydrol 617. https://doi.org/10.1016/j.jhydrol.2022.128992

Monteiro JAF, Strauch M, Srinivasan R, Abbaspour K, Gücker B (2016) Accuracy of grid precipitation data for Brazil: application in river discharge modelling of the Tocantins catchment. Hydrol Process 30(9):1419–1430. https://doi.org/10.1002/hyp.10708

Nash JE, Sutcliffe JV (1970) River flow forecasting through conceptual models part I – a discussion of principles. J Hydrol 10(3):282–290

Oeurng C, Sauvage S, Sanchez-Perez JM (2011) Assessment of hydrology, sediment and particulate organic carbon yield in a large agricultural catchment using the SWAT model. J Hydrol 401:145–153 (4–3. https://doi.org/10.1016/j.jhydrol.2011.02.017

Park CK, Byun HR, Deo R, Lee BR (2015) Drought prediction till 2100 under RCP 8.5 climate change scenarios for Korea. J Hydrol 526:221–230. https://doi.org/10.1016/j.jhydrol.2014.10.043

Porhemmat J, Nakhaei M, Dadgar MA, Biswas A (2018) Investigating the effects of irrigation methods on potential groundwater recharge, case study: semiarid regions in Iran. J Hydrol 565:455–466. https://doi.org/10.1016/j.jhydrol.2018.08.036

Prudhomme C, Reynard N, Crooks S (2002) Downscaling of global climate models for flood frequency analysis: where are we now? Hydrol Process 16(6):1137–1150. https://doi.org/10.1002/hyp.1054

Prudhomme C, Jakob D, Svensson C (2003) Uncertainty and climate change impact on the flood regime of small UK catchments. J Hydrol 277(1–2):1–23. https://doi.org/10.1016/S0022-1694(03)00065-9

Rasco P, Szeidl L, Semenov MA (1991) A serial approach to local stochastic models. Ecol Model 57(1–2):27–41. https://doi.org/10.1016/0304-3800(91)90053-4

Rostamian R, Jaleh A, Afyuni M, Mousavi SF, Heidarpour M, Jalalian A, Abbaspour KC (2008) Application of a SWAT model for estimating runoff and sediment in two mountainous basins in central Iran. J Hydrol 53(5):977–988. https://doi.org/10.1623/hysj.53.5.977

Santini M, Paola AD (2015) Changes in the world rivers' discharge projected from an updated high resolution dataset of current

and future climate zones. J Hydrol 531:768–780. https://doi.org/10.1016/j.jhydrol.2015.10.050

Schuo J, Abbaspour KC (2007) Using monthly weather statistics to generate daily data in a SWAT model application to West Africa. Ecol Model 201(3–4):301–311. https://doi.org/10.1016/j.ecolmodel.2006.09.028

Semenov MA, Barrow EA (2002) LARS-WG a stochastic weather generator for use in climate impact studies. User's manual

Sommerlot AR, Nejadhashemi A, Woznicki SA, Giri S, Prohaska MD (2013) Evaluating the capabilities of watershed-scale models in estimating sediment yield at field-scale. J Environ Manage 127:227–236. https://doi.org/10.1016/j.jenvman.2013.05.018

Su B, Zeng X, Zhai J, Wang Y, Li X (2015) Projected precipitation and streamflow under SRES and RCP emission scenarios in the Songhuajiang River basin, China. Quatern Int 380–381. https://doi.org/10.1016/j.quaint.2014.03.049

Te Linde AH, Aerts JC, Hurkmans RT, Eberle M (2008) Comparing model performance of two rainfall-runoff models in the Rhine basin using different atmospheric forcing data sets. Hydrology Earth System Sci 12:943–957, https://doi.org/10.5194/hess-12-943-2008

Van Vuuren DP, Edmonds J, Kainuma M, Riahi K, Thomson A, Hibbard K, and Rose S. K (2011) The representative concentration pathways: an overview. Clim Change 109:5–31. https://doi.org/10.1007/s10584-011-0148-z

Verbeeten E, Barendregt A (2007) The impacts of climate change on hydrological services provided by dry forest ecosystems. In: West Africa, 4th International SWAT Conference

Wilby RL, Harris I (2006) A framework for assessing uncertainties in climate change impacts: low flow scenarios for the River Thames, UK. Water Resour Res 42(2):1–10

Yang J, Reichert P, Abbaspour KC, Yang H (2017) Hydrological modelling of the Chaohe Basin in China: statistical model formulation and bayesian inference. J Hydrol 340(3–4):167–182. https://doi.org/10.1016/j.jhydrol.2007.04.006

Zuo D, Xu Z, Yao W, Jin S, Xiao P, Ran D (2016) Assessing the effects of changes in land use and climate on runoff and sediment yields from a watershed in the Loess Plateau of China. Sci Total Environ 544:238–250. https://doi.org/10.1016/j.scitotenv.2015.11.060